

Distributed optical fiber sensors for integrated monitoring of railway infrastructures

Aldo Minardo^{*1}, Agnese Coscetta¹, Giuseppe Porcaro², Daniele Giannetta³,
Romeo Bernini⁴ and Luigi Zeni¹

¹*Department of Industrial and Information Engineering, Second University of Naples,
Via Roma 29 Aversa, Italy*

²*Tecnomatica SaS, Corso del Mezzogiorno III trav. 71122 Foggia, Italy*

³*Ferrovie del Gargano, Direzione di Esercizio – 71016 San Severo - Foggia, Italy*

⁴*Istituto per il Rilevamento Elettromagnetico dell'Ambiente – Consiglio Nazionale delle Ricerche,
Via Diocleziano, 328 – 80124 Napoli, Italy*

(Received February 7, 2014, Revised May 28, 2014, Accepted May 30, 2014)

Abstract. We describe the application of a distributed optical fiber sensor based on stimulated Brillouin scattering, as an integrated system for safety monitoring of railway infrastructures. The strain distribution was measured statically and dynamically along 60 meters of rail track, as well as along a 3-m stone arch bridge. We show that, gluing an optical fiber along the rail track, traffic monitoring can be performed in order to identify the train passage over the instrumented sector and determine its running conditions. Furthermore, dynamic and static strain measurements on a rail bridge are reported, aimed to detect potential structural defects. The results indicate that distributed sensing technology represents a valuable tool in railway traffic and safety monitoring.

Keywords: optical fiber measurements; brillouin scattering; structural health monitoring

1. Introduction

The demand for safe and cost-effective train operation in the railroad transportation industry has dramatically increased in the last years. An efficient railway maintaining and inspection technique may provide information about the rail and wheel defects (Nielsen and Johansson 2000, Wilcox *et al.* 2003, Lee *et al.* 2009, Rizzo *et al.* 2010). In the field of railway infrastructure monitoring, structural health monitoring (SHM) is a key element of industrial businesses. Standard inspection techniques may fail in revealing defects or unusual features, and some components may not receive close up examination if, for example, access is difficult or operating conditions do not permit. Distributed optical fiber sensing techniques allow distributed temperature and strain measurements to be captured in real time over lengths of a few meters to tens of kilometers (Bao and Chen 2011). A permanently installed optical fiber provides continuous information about the status of the structure during its whole life cycle, thereby offering a unique opportunity in long-term SHM (Minardo *et al.* 2012, Ko and Ni 2005).

*Corresponding author, Professor, E-mail: aldo.minardo@unina2.it



Fig. 1 Map of the Peschici–San Severo regional railway line. The marks (a) and (b) indicate the two stations closest to the site chosen for the test campaigns. a: Rodi Station; b: Peschici Station (map data © 2013 Google)

Also, distributed sensors are able to acquire in real time the deformation of the rail track and infrastructures induced by train passage. Analyzing the dynamic deformation several parameters can be retrieved simultaneously, such as axle counting, speed monitoring and dynamic load (Minardo *et al.* 2013, Duan *et al.* 2014), and to identify weaknesses in the infrastructures, as well.

In this work, we report static and dynamic strain measurements performed by using a Brillouin Optical Time-Domain Analysis (BOTDA) interrogation unit developed by our group. The tests were performed on the Peschici–San Severo regional railway line, connecting the northern coast of Gargano to the Adriatic railway, and operated by Ferrovie del Gargano. In particular, dynamic tests were performed along a 60 m rail sector, as well as a stone bridge located in proximity of the San Menaio Station (see Fig. 1). Also, we report the results of a 15-months monitoring campaign performed on the same railway bridge. Such activity was aimed to reveal the onset of potential structural damages of the bridge.

2. Operation principle

When a lightwave is propagated in an optical fiber, some portions of the incident light are scattered due to changes in density and composition, as well as molecular and bulk vibrations. The scattered light consists of different spectral components around the original frequency, due to different interaction mechanisms between the propagating light wave and the medium. In optical fibers, Brillouin scattering arises from acoustic waves guided in the optical fiber. When a pump wave and a frequency down-shifted counter-propagating probe wave are simultaneously injected into the fiber, their interference generates an acoustic wave through electrostriction, and the Bragg diffraction induced by the acoustic wave subsequently scatters the pump wave into the probe wave. This process is responsible for the energy transfer that leads to a gain in the probe wave through the energy loss in the pump wave. Maximum probe gain occurs for a definite value of the pump-probe frequency shift, named Brillouin frequency shift, which depends on the strain and the temperature variation applied to the optical fiber (Niklès *et al.* 1997).

The BOTDA is a method that generates Brillouin gain at a specified location along the optical

fiber, by pulsing the intensity of the pump wave. Probe amplification is recorded as a function of time, since the instant of launch of the pulsed pump, for a selected numbers of pump-probe frequency shifts. Acquisition time is then converted in fiber locations, by using the group velocity of the pump. Standard BOTDA method offers good accuracy and long sensing range. However, its acquisition speed is limited due to the necessity to scan the pump-probe frequency shift. When a high (> 1 Hz) acquisition rate is needed, a variant of the BOTDA method, the so-called slope-assisted BOTDA (Bernini *et al.* 2009, Peled *et al.* 2013) can be used, in which the pump-probe frequency shift is kept fixed at the mid-gain point of the Brillouin spectrum. By this way, the Brillouin frequency shift modulation produced by dynamic strain is acquired at high speed by recording the related modulation of the probe intensity. The maximum acquisition rate allowed by this method is related to the fiber length, via the round-trip time of the pulsed pump. For example, for a fiber length of 100 m the round trip time is 1 μ s, resulting in a maximum acquisition rate of 1 MHz. In practical cases, the maximum acquisition rate is usually limited to a few tens of Hz, due to the need of averaging a sufficient number of traces.

3. Results of dynamic strain measurements along the rail track

Dynamic strain was acquired along a standard telecommunications single-mode optical fiber with an overall diameter of 900 μ m, glued along a 60-m rail sector by use of epoxy adhesive. Details on the installation procedure can be found in the publication (Minardo *et al.* 2013). When the train passes over the instrumented rail, the weight of each axle induces a deformation on the rail itself, which is transferred to the optical fiber. If the latter is disposed below the neutral axis of the rail, a localized, tensile strain peak is recorded by the sensor at each axle passage. Therefore, axle counting can be easily performed by counting the number of strain peaks associated to the passing train, provided that the acquisition rate is sufficiently large (Filograno *et al.* 2012, Kerrouche *et al.* 2009). Furthermore, a dynamic strain temporal waveform is retrieved for each sensed position, thereby offering the opportunity to retrieve other pieces of information such as axle spacing and train speed (Minardo *et al.* 2013).

We show in Fig. 2(a) the dynamic strain captured by the slope-assisted BOTDA sensor at a spatial resolution of 1 m and an acquisition rate of 31 profiles/s, when the instrumented rail sector is crossed by a two-bogies (four axles) train bound for Rodi. The measurement was done during commercial service of the railway line. Four diagonal lines are distinguished in the measured strain map, each one associated to a specific train axle. Fig. 2(b) shows the dynamic strain measured at a specific location ($z = 48$ m). It is seen that each axle induces a tensile strain of ~ 200 μ ϵ when crossing the selected position. As the axle traces appearing in Fig. 2(a) are straight lines, it is easily concluded that the train was running at constant speed during its passage over the instrumented rail. Actually, the speed of each axle coincides with the slope of the corresponding strain trace. By fitting a straight line to any of the traces in Fig. 2(a), a speed of 39.5 km/h is retrieved for the passing train.

As a second test, we recorded the strain footprint left by a diagnostic car. The latter was composed of a two-bogies (four axles) motor car, followed by two trailer cars, each one composed of two bogies. Differently from the previous case, the diagnostic car was not performing commercial service. Therefore, the measurement could be performed in a special condition, in which the train, bound for Rodi, was accelerating when crossing the monitored sector.

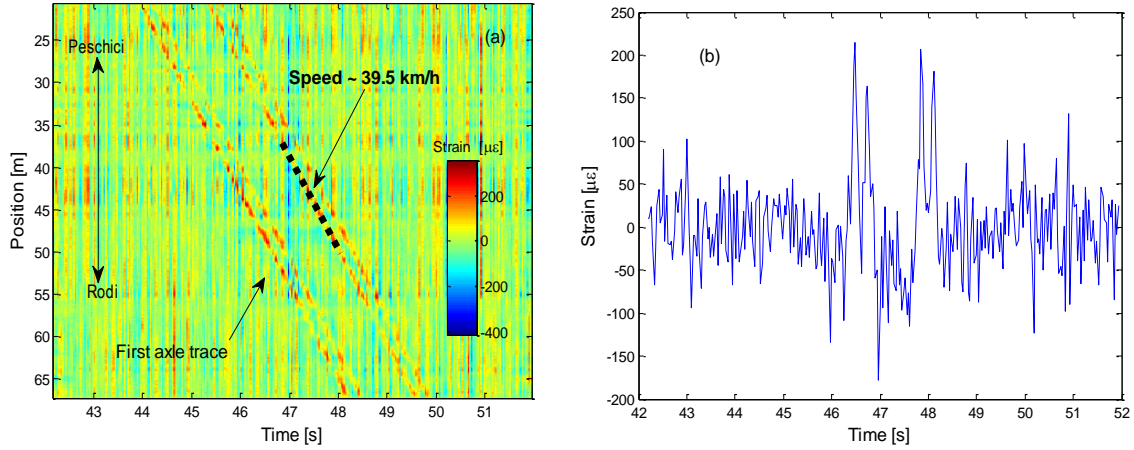


Fig. 2 (a) Strain induced on the rail track by train passage as a function of time and position; (b) Strain induced by train passage as a function of time, at $z = 48$ m

The result of the acquisition, still performed at 1 m spatial resolution and 31 profiles/s acquisition rate is shown in Fig. 3. Note that the positions corresponding to the fiber portion attached to the rail range from $z \sim 12$ m to $z \sim 72$ m. Carefully examining the strain map, up to six bogies (12 axles) are recognized, two of them belonging to the motor car ((e-f)), the other four to the trailer cars ((a-d)). We also observe that the axle traces are not straight lines, rather they show some curvature. A curvature in our space-time representation is a clear sign of acceleration. In particular, the measurements indicate a positive acceleration of the train during its passage over the monitored sector. Note that, along the very first meters of the instrumented rail (from $z \sim 12$ m to $z \sim 20$ m), the slopes of the various axles are not uniform, instead they increase when moving from bogie (f) to bogie (a). This is due to the fact that, while the car is accelerating, the driving motor car moves at higher speed than the two trailer cars, as it is also demonstrated by the fact that the axle traces become increasingly closer during the measurement interval. It is also interesting to observe that the strain associated to the last trailer car (bogies (a) and (b)) induces a larger deformation than the other two cars, although all the cars have the same nominal static load (50 t). This is a quite obvious consequence of the fact that the train is accelerating, resulting in a load transfer from front to rear axles.

For demonstration purposes, we report the calculation of the speed for one of the axles. In particular, we chose the first axle (i.e., the first one entering the instrumented section) as it was the one experiencing the maximum acceleration. Axle trace was retrieved by identifying the time instant at which the strain peak is visible on the acquired traces, at each fiber position. The results of this procedure are reported in Fig. 4(a) (solid blue line). The axle speed is then computed by taking the slope of the retrieved trace in each point. In order to avoid large errors in speed calculation, the axle trace shown in Fig. 4(a) was first fitted with a fourth-order polynomial curve (read dashed line in Fig. 4(a)). Therefore, the axle speed was calculated by taking the first derivative of the fitted curve. The result is reported in Fig. 4(b), confirming that the axle is accelerating during the measurement interval.

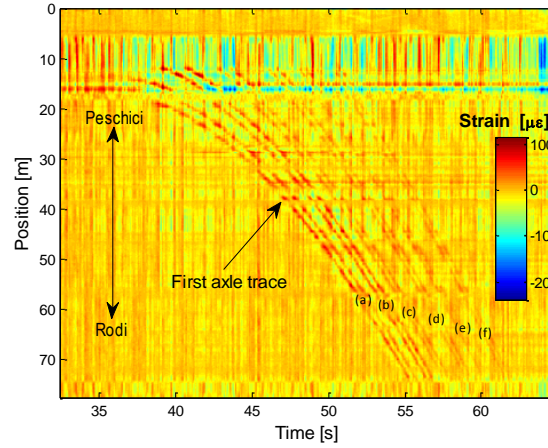


Fig. 3 Strain induced on the rail track by diagnostic car passage as a function of time and position. The letters from (a) to (f) indicate the six bogies of the train

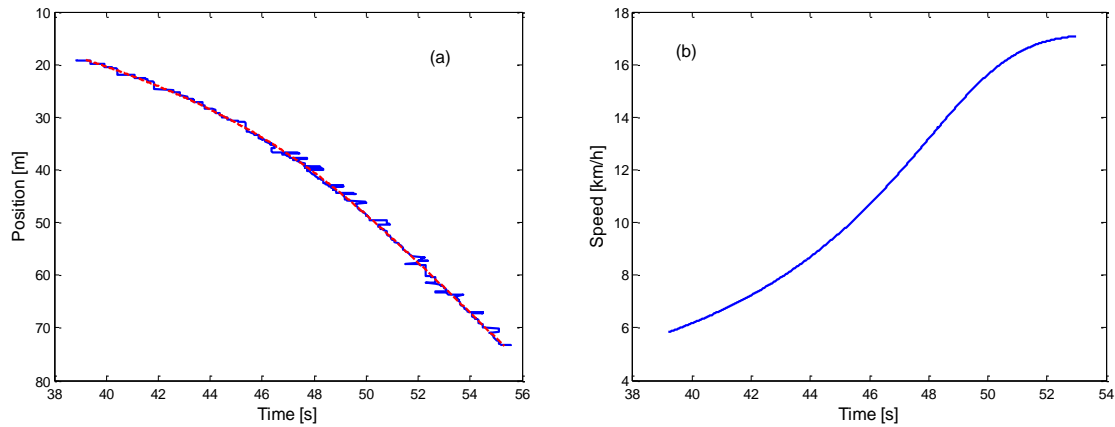


Fig. 4 (a) Axle trace relative to the first axle, as retrieved from data shown in Fig. 3. The red dashed line is the 4-th order polynomial fit, with coefficient of determination $R^2=0.9983$. (b) Speed of the first axle as a function of time, computed by deriving the polynomial fit

Another test was carried out to reveal the temperature-induced Brillouin shift variation along the fiber bonded to the rail. Actually, in the slope-assisted BOTDA method it is essential to select a pump-probe frequency shift placed on the slope of the Brillouin spectrum, except from the case in which a specially synthesized probe wave is used (Peled *et al.* 2011). As the Brillouin gain spectrum shifts with temperature, it is important to estimate the changes of Brillouin frequency shift with temperature. In order to get a reference temperature, we also measured the Brillouin frequency shift along another piece of fiber identical to the attached one, disposed near the track but not glued to it. Measurements were done during a 7-hour interval, in order to record a sufficiently wide temperature excursion. We show in Fig. 5 the evolution of the Brillouin shift

along the bonded and not-bonded fiber, acquired by operating the BOTDA instrument at 1-m spatial resolution. Note that the Brillouin shifts reported in Fig. 5 refer to the average values along the two fiber strands. While the offset between the two curves should be attributed to the strain induced by the gluing procedure, the overall Brillouin shift variation is about 21.0 MHz for the free fiber, and about 29.4 MHz for the attached one. In other terms, the glued fiber strand experiences a wider Brillouin shift variation, compared to the free fiber.

By plotting the Brillouin frequency shift along the bonded fiber, as a function of the corresponding Brillouin shift along the free fiber (see Fig. 5(b)), a slope coefficient of ~ 1.35 is retrieved. In other words, the temperature-induced Brillouin shift variation along the glued fiber was about 35% larger than the corresponding variation along the free segment. Actually, while the Brillouin frequency shift in both fibers varies with temperature with a slope of ~ 1.05 MHz/ $^{\circ}$ C (as determined by laboratory calibration), the glued fiber is also subjected to thermal apparent strain, which arises from the different thermal expansion coefficients of rail track material (steel) and optical fiber (fused silica). Using a thermal expansion coefficient for silica and steel equal to $0.55 \cdot 10^{-6}/^{\circ}$ C and $12.0 \cdot 10^{-6}/^{\circ}$ C, respectively, the thermal strain may be estimated as (Valis *et al.* 1992)

$$\varepsilon_{thermal} = (12.0 - 0.55) \mu\varepsilon/^{\circ}\text{C} = 11.45 \mu\varepsilon/^{\circ}\text{C} \quad (1)$$

By assuming a Brillouin shift / strain sensitivity of 403 MHz/% (as determined by laboratory calibration), the thermal strain should produce an additional ~ 0.46 MHz/ $^{\circ}$ C variation of Brillouin frequency shift, which corresponds to a 44% increase of thermal sensitivity with respect to the free fiber. The predicted factor is quite larger than the 35% factor observed experimentally. A possible cause of discrepancy is a not completely free expansion/contraction of the rail track under temperature changes. Actually, the rail track is not an isolated element, rather it is influenced by other elements such as fasteners, ballast, etc. which prevent the rail track to freely expand or contract under temperature changes.

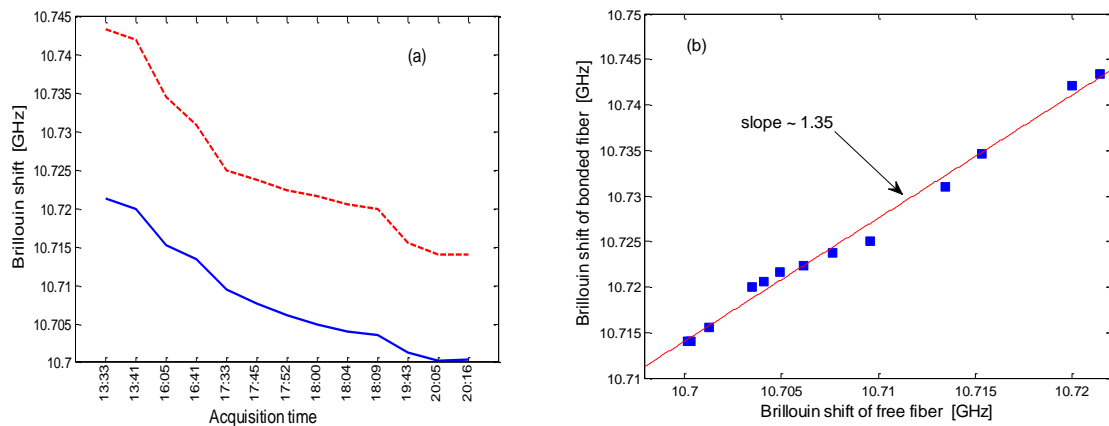


Fig. 5 (a) Average Brillouin frequency shift of free fiber (blue solid line) and glued fiber (red dashed line). (b) Brillouin frequency shift along the glued fiber versus Brillouin frequency shift along the free fiber (squares). The red line is the linear fit, with coefficient of determination $R^2 = 0.9908$

4. Results of dynamic and static strain measurements along the rail bridge

The second test campaign was performed on a railway bridge located close to the instrumented rail sector (San Menaio Station). The bridge is a 3 m-long, single span, stone arch bridge, showing evident signs of ageing.



Fig. 6 Instrumented rail bridge (picture of “sea side”). The red curves indicate the path of the glued optical fiber

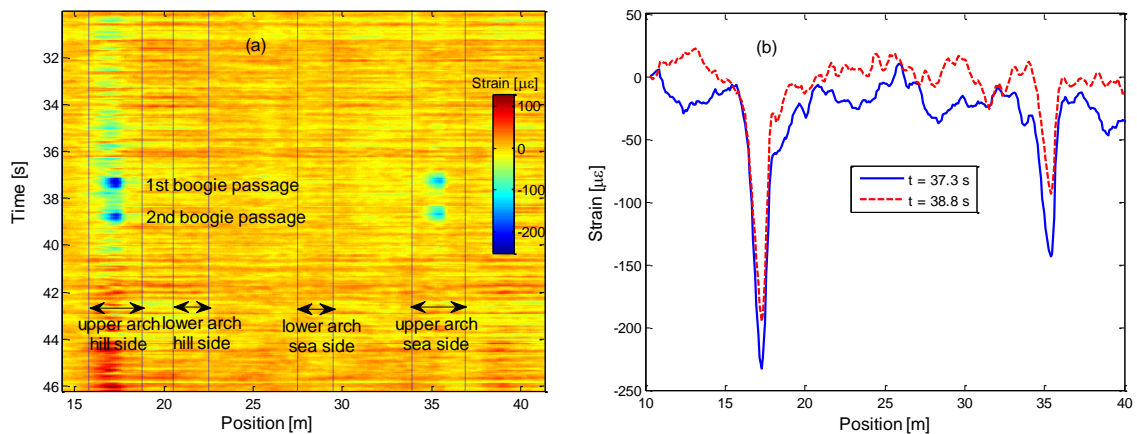


Fig. 7 (a) Strain induced on the arch bridge by train passage, as a function of time and position; (b) Strain induced on the arch bridge by train passage as a function of position, at $t = 9.27$ s (blue solid line) and $t = 10.75$ s (red dashed line).

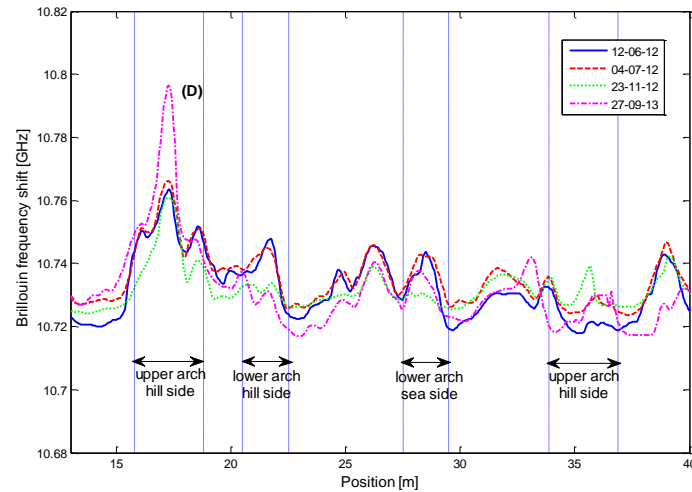


Fig. 8 Brillouin frequency shift profile measured along the fiber installed on the rail bridge. The vertical lines delimit, approximately, the fiber strands attached to the bridge. The region marked with D refers to an anomalous increase of the Brillouin shift detected in the last acquisition. The inset shows a picture of the middle part of the arch (“hill” side)

In order to perform SHM, a piece of single-mode standard fiber, identical to the one employed in the previous tests, was glued directly over the bridge following four paths, two of them are highlighted in Fig. 6. The other two paths are identical to those shown in Fig. 6, but lied on the opposite side of the bridge. In order to distinguish the various fiber paths, we refer to them as “upper arch” and “lower arch”, and “sea side” (that shown in Fig. 6) and “hill side” (the opposite side). As far as the dynamic test is concerned, the measurements, carried out at 1 m spatial resolution and 43 profiles/s acquisition rate, were performed on 23 November 2012, when a two-bogies (four axles) train was passing over the bridge. The results, summarized in Fig. 7(a), show that two definite, compressive strain peaks appear along the fiber at the passage of each bogie. In particular, the two peaks were recorded around the middle of the two fiber strands glued along the upper part of the arch, with the most compressed one lying on the “hill side”. Mapping the two fiber positions on the monitored structure, these two sections correspond approximately to the upper part of the arch keystone. Fig. 7(b) reports the strain acquired at the instants in which the two train bogies pass over the bridge.

As far as the long term static monitoring is concerned, we performed four measurements of the Brillouin frequency shift distribution, at 1-m spatial resolution, in a period comprised between June 2012 and September 2013. The results are shown in Fig. 8. Apart from some vertical offset between the various profiles, which is attributed to ambient temperature, an anomalous peak is identified in the last acquired Brillouin frequency shift distribution (Sept 2013) (it is denoted as D). As it can be seen from the comparison with the dynamic measurements, the anomalous peak appears, approximately, at the same bridge section on which the largest compressive peak was observed during the train passage (upper part of the arch keystone, “hill side” path).

Comparing the last two static acquisitions, the maximum change of the Brillouin shift in D was ~ 35 MHz, corresponding to a strain increase of $\sim 870 \mu\epsilon$. Apparently, an already existing or a new crack has been opening around the monitored section, which is detected by the sensor as a local

increase of the Brillouin frequency shift (Minardo *et al.* 2012). Such an occurrence was also verified by visual inspection. Actually, the wall of the arch bears an externally-visible diagonal crack, running from the base up to the top of the arch. While the revealed defect at its present state does not compromise the safe and proper operation of the railway line, the damaged section is now monitored on a regular basis by the regional line operator.

5. Conclusions

A fiber-optic distributed sensor has been employed for integrated monitoring of railway infrastructures. The sensor is based on stimulated Brillouin scattering in an optical fiber. The slope-assisted BOTDA method was employed for fast, distributed strain measurements. The results indicate that, gluing an optical fiber along the rail, traffic monitoring can be performed in order to identify the train passage over the instrumented sector and determine its running conditions. Furthermore, dynamic and static strain measurements on a rail bridge have been performed, aimed to detect potential structural defects.

It is believed that health monitoring systems based on distributed optical fiber technology can offer valuable information in evaluating structural integrity, durability and reliability, and in ensuring optimal maintenance planning and safe operation.

In order to make the system applicable over longer rail sectors, an automated fiber installation cart should be developed, by which the fiber placement and bonding process on the rail is carried out at a high application rate. Also, the optical fiber should be installed in such a way to avoid exposition to disturbances such as rain and wind, which may compromise, over time, the mechanical coupling between the rail and the fiber.

Acknowledgments

The research leading to the results in this work was supported by the European Community's Seventh Framework Program (FP7/2007–2013) under Grant Agreement 265954. The authors acknowledge support from the European COST action TD1001–OFSESA.

References

- Bao, X. and Chen, L. (2011), "Recent progress in Brillouin scattering based fiber sensors", *Sensors*, **11**, 4152-4187.
- Bernini, R., Minardo, A. and Zeni, L. (2009), "Dynamic strain measurement in optical fibers by stimulated Brillouin scattering", *Opt. Lett.*, **34**(17), 2613-2615.
- Duan, N., Peng, F., Rao, Y.J., Du, J. and Lin, Y. (2014), "Field test for real-time position and speed monitoring of trains using phase-sensitive optical time domain reflectometry (Φ -OTDR)", *Proceedings of the 23rd International Conference on Optical Fibre Sensors*, (Eds., José Miguel López-Higuera, Julian Jones, Manuel López-Amo, José Luis Santos), Proc. of SPIE, **9157**, 91577A, doi: 10.1117/12.2059188.
- Filigrano, M.L., Corredera Guillen, P., Rodriguez-Barrios, A., Martin-Lopez, S., Rodriguez-Plaza, M., Andres-Alguacil, A., Gonzalez-Herraez, M. (2012), "Real-time monitoring of railway traffic using fiber bragg grating sensors", *IEEE Sens. J.*, **12**, 85-92.
- Kerrouche, A., Boyle, W.J.O., Sun, T. and Grattan, K.T.V. (2009), "Design and in-the-field performance

- evaluation of compact FBG sensor system for structural health monitoring applications”, *Sens. Actuat. A - Phys.*, **151**(2), 107-121.
- Ko, M. and Ni, Y.Q. (2005), “Technology developments in structural health monitoring of large-scale bridges”, *Eng. Struct.*, **27**(12), 1715-1725.
- Lee, C.M., Rose, J.L. and Cho, Y. (2009), “A guided wave approach to defect detection under shelling in rail”, *NDT & E Int.*, **42**(3), 174-180.
- Minardo, A., Bernini, R., Amato, L. and Zeni, L. (2012), “Bridge monitoring using Brillouin fiber-optic sensors”, *IEEE Sens. J.*, **12**(1), 145-150.
- Minardo, A., Porcaro, G., Giannetta, D., Bernini, R. and Zeni, L. (2013), “Real-time monitoring of railway traffic using slope-assisted Brillouin distributed sensors”, *Appl. Optics.*, **52**(16), 3770-3776.
- Nielsen, J.C.O. and Johansson, A. (2000), “Out-of-round railway wheels-a literature survey”, *Proceedings of the Institution of Mechanical Engineers, Part F: J. Rail and Rapid Transit*, **214**(2), 79-91.
- Niklès, M., Thévenaz, L. and Robert, P.A. (1997), “Brillouin gain spectrum characterization in single-mode optical fibers”, *IEEE J. Lightw. Technol.*, **15**(10), 1842-1851.
- Peled, Y., Motil, A., Yaron, L. and Tur, M. (2011), “Slope-assisted fast distributed sensing in optical fibers with arbitrary Brillouin profile”, *Opt. Express.*, **19**(21), 19845-19854.
- Peled, Y., Motil, A., Kressel, I. and Tur, M. (2013), “Monitoring the propagation of mechanical waves using an optical fiber distributed and dynamic strain sensor based on BOTDA”, *Opt. Express.*, **21**(9), 10697-10705.
- Rizzo, P., Cammarata, M., Bartoli, I., Lanza di Scalea, F., Salamone, S., Coccia, S. and Philips R. (2010), “Ultrasonic guided waves-based monitoring of rail head: laboratory and field tests”, *Adv. Civil Eng.*, **210**, <http://dx.doi.org/10.1155/2010/291293>.
- Valis, T., Hogg, D., Measures, R.M. (1992), “Thermal apparent-strain sensitivity of surface-adhered, fiber-optic strain gauges”, *Appl. Optics.*, **31**(34), 7178-7179.
- Wilcox P., Pavlakovic B., Evans M., Vine K., Cawley P., Lowe M., Alleyne D. (2003), “Long range inspection of rail using guided waves”, *Rev. Prog. Quant. Nondestruct. Eval.*, **22**, 236-243.